Competitive Binding of Acetate and Chloride in Photosystem II†

Henriette Kühne,‡ Veronika A. Szalai,§,|| and Gary W. Brudvig*,§

Department of Chemistry, P.O. Box 208107, and Department of Molecular Biophysics & Biochemistry, P.O. Box 208114, Yale University, New Haven, Connecticut 06520

Received February 11, 1999

ABSTRACT: The binding of chloride and acetate to photosystem II (PSII) was examined to elucidate the mechanism of acetate inhibition. The mode of inhibition was studied, and individual binding sites were assigned by steady-state O_2 evolution measurements in correlation with electron paramagnetic resonance (EPR) results. Two binding sites were found for acetate, one chloride-sensitive on the electron donor side and one chloride-insensitive on the electron acceptor side. The respective binding constants were as follows: $K_{Cl} = 0.5 \pm 0.2$ mM (chloride binding to the donor side), $K_I = 16 \pm 5$ mM (acetate binding to the donor side), and $K_I' = 130 \pm 40$ mM (acetate binding to the acceptor side). When acetate was bound to the acceptor side of PSII, 200 K illumination induced a narrowed form of the $Q_A^-Fe^{II}$ EPR signal, the yield of which was independent of the chloride concentration. When acetate was bound to the donor side, room-temperature illumination produced the $S_2Y_Z^\bullet$ state. EPR measurements showed that both the yield and formation rate of this state increased with acetate concentration. Increasing chloride concentrations slowed the rate of formation of the $S_2Y_Z^\bullet$ state, but did not affect the steady-state yield of the $S_2Y_Z^\bullet$ state. These findings indicate that the light-induced reactions in acetate-inhibited PSII are modulated by both donor side and acceptor side binding of acetate, while the steady-state yield of the $S_2Y_Z^\bullet$ state at the high PSII concentrations used for EPR measurements depends primarily on acceptor side turnover. Our data further support a close proximity of chloride to $Y_Z^\bullet$, indicating a possible role for chloride in the electron-transfer mechanism at the O_2-evolving complex.

Photosystem II (PSII[1]), an integral membrane protein complex in chloroplast thylakoid membranes, carries out the initial steps in oxygenic photosynthesis. As photons are absorbed, electrons are transferred from the central chlorophyll, P680, to the iron−quinone site at the electron acceptor side of the enzyme, while reducing equivalents are supplied from the O_2-evolving complex (OEC) at the electron donor side. With successive photochemical charge separations, the OEC cycles through a series of oxidation states called S_i states ("store" states, $i = 0-4$), first proposed by Kok et al. (*1*). Molecular oxygen is released from the OEC during the S_4-to-S_0 transition (*2*). The OEC contains a tetramanganese (Mn_4) cluster, which has been postulated to consist of a dimer of μ-oxo-bridged dimers (*3*), and a closely associated redox-active tyrosine, Y_Z. The structure of the Mn_4-Y_Z ensemble is being debated, and the details of the water oxidation mechanism remain unknown.

Calcium and chloride are required for maximum O_2 evolution activity in PSII. The number and location of chloride ions bound to PSII have been difficult to determine (*2*, *4*−*6*). Studies of PSII isolated from spinach grown on ^{36}Cl have shown that one chloride per PSII is tightly bound in the dark and exchanges slowly, as long as the site is unperturbed (*7*). Depending on the method of chloride removal, this high-affinity site may be converted to a low-affinity site (*8*−*10*). The observation of low- or high-affinity chloride binding may be controlled by the presence of the 17 and 23 kDa extrinsic polypeptides which provide a barrier to diffusion (*11*).

Evidence that chloride is bound near the OEC is provided by the fact that chloride-depleted PSII membranes exhibit altered S_2-state EPR signals (*12*) and that chloride is required for the S_2-to-S_3 transition (*13*). In addition, chloride-depleted PSII samples display a broadened radical EPR signal centered at $g = 2.0$ when illuminated at temperatures above 250 K and quickly cooled to 77 K (*14*−*16*). This signal is attributed to the $S_2Y_Z^\bullet$ state (*17*−*19*) which accumulates under steady-state illumination because of the requirement for chloride in the S_2-to-S_3 transition (*13*). Acetate-inhibited PSII also displays an $S_2Y_Z^\bullet$ EPR signal following illumination at temperatures at or above 250 K (*20*−*22*), indicating that acetate and chloride binding to the OEC may be related.

The $S_2Y_Z^\bullet$ EPR signal arises from the coupling of the electron spins of the Mn_4 cluster and $Y_Z^\bullet$. Analysis of these spin−spin interactions has inspired much interest recently because they provide information about the structural relationship between the Mn_4 cluster and $Y_Z^\bullet$. The $S_2Y_Z^\bullet$ EPR

† This work was supported by the National Institutes of Health (Grant GM32715) and a predoctoral traineeship to V.A.S. (GM08283).

* To whom correspondence should be addressed. Phone: (203) 432-5202. Fax: (203) 432-6144. E-mail: gary.brudvig@yale.edu.

‡ Department of Molecular Biophysics & Biochemistry.

§ Department of Chemistry.

|| Current address: Department of Chemistry, University of North Carolina at Chapel Hill, Chapel Hill, NC 27599-3290.

[1] Abbreviations: CW, continuous wave; DMSO, dimethyl sulfoxide; EPR, electron paramagnetic resonance; MES, 2-(*N*-morpholino)-ethanesulfonic acid; OEC, O_2-evolving complex; P680, photoactive chlorophyll dimer in PSII; PPBQ, phenyl-*p*-benzoquinone; PSII, photosystem II; Q_A, tightly bound quinone in PSII; Q_B, exchangeable quinone in PSII; Y_D, redox-active tyrosine 160 of the D2 polypeptide; Y_Z, redox-active tyrosine 161 of the D1 polypeptide.

10.1021/bi990341t CCC: $18.00
Published on Web 04/28/1999

signal generated in acetate-inhibited PSII is unique because both the component S_2 state and $Y_Z^\bullet$ EPR signals are observable (*20*−*22*). For this reason, acetate-inhibited PSII has become a valuable system for studying the structure of the OEC (*20*−*28*). It has been proposed that acetate binding to the OEC prevents S-state advance past S_2 by blocking proton-coupled electron transfer to $Y_Z^\bullet$ (*23*). Several previous studies have attributed formation of the $S_2Y_Z^\bullet$ EPR signal in acetate-inhibited PSII to replacement of chloride by acetate (*20*−*22*). If this is the case, EPR studies of the $S_2Y_Z^\bullet$ state in acetate-inhibited PSII may provide insight into chloride's location near the Mn_4 cluster and its role in OEC function. However, clarification of the mechanism of acetate inhibition is needed to justify the use of the $S_2Y_Z^\bullet$ state in acetate-inhibited PSII as a spectroscopic probe of the donor side chloride-binding site and of the OEC. In this study, binding of chloride and acetate to PSII is characterized by steady-state O_2 evolution activity assays in correlation with EPR measurements.

When the O_2 evolution activity was examined at two chloride concentrations and in the presence of acetate, the inhibitory effects of acetate were found to depend on the chloride concentration (*29*, *30*). Inhibition of O_2 evolution in the presence of nucleophiles has been attributed to competitive exchange of one nucleophile for another into an electrophilic site usually occupied by chloride (*30*−*32*). For either structural or electronic reasons, anions other than chloride or bromide cannot support O_2 evolution. Bromide is the only anion which can functionally replace chloride both in O_2 evolution experiments and in low-temperature EPR experiments (*11*, *33*, *34*). Steady-state O_2 evolution measurements demonstrating that certain inhibitors bind in competition with chloride have been performed for fluoride, ammonia, and some amines (*30*−*32*, *35*, *36*).

Many inhibitory anions bind not only to the donor side but also to the non-heme iron on the acceptor side of PSII. In the bacterial reaction center, the non-heme iron is ligated by four histidine residues and one bidentate glutamate residue (*37*). Although the four ligating histidines are conserved in PSII, the remaining coordination sites on the iron may not be occupied by amino acid side chains. Bicarbonate, which has long been known to be required for maximum O_2 evolution (*38*−*40*), has been suggested to serve as a ligand to the non-heme iron in PSII (*37*). Other exogenous ligands bind to or near the non-heme iron in PSII in competition with bicarbonate. They include nitric oxide (*41*, *42*), cyanide (*43*), and carboxylic acids such as formate, oxalate, and malate (*44*−*46*).

The binding of carboxylic acids to or near the non-heme iron alters the *g* value and shape of the associated $Q_A^-Fe^{II}$ EPR signal (*44*, *45*) and slows the rate of electron transfer from Q_A^- to Q_B (*46*). High concentrations of acetate also impede Q_A^--to-Q_B electron transfer (*47*, *48*), presumably by competing with bicarbonate for an acceptor side binding site (*40*, *49*). In addition, acetate-inhibited PSII produces a sharpened and shifted $Q_A^-Fe^{II}$ EPR signal characteristic of a change in the geometry and/or ligation of the non-heme Fe^{II} (*20*, *21*).

The aims of this study are to examine the mode of acetate inhibition through steady-state O_2 evolution activity assays and to link the EPR signals from the S_2 and $S_2Y_Z^\bullet$ states of acetate-treated PSII to the acetate-binding site(s) observed by steady-state O_2 evolution measurements. Steady-state O_2 evolution rates measured at a range of acetate and chloride concentrations show that acetate binds to PSII in linear mixed competition with chloride. Comparisons are drawn to ammonia binding studies (*30*−*32*, *50*, *51*) and to the EPR signals induced by various inhibitory treatments of the donor side (*20*−*28*), as well as by binding of carboxylic acids to the acceptor side (*40*, *42*, *44*−*46*, *49*). Low-temperature and room-temperature EPR experiments confirm the existence of at least two acetate-binding sites, pointing to a chloride-insensitive acetate-binding site on the acceptor side and a chloride-sensitive acetate-binding site on the donor side of PSII. On the basis of the steady-state O_2 evolution activity and EPR measurements, we present a model in which acetate binds to the OEC in competition with chloride and to the non-heme iron independently of chloride. We further discuss possible mechanisms for chloride and acetate binding to or near the Mn_4 cluster.

EXPERIMENTAL PROCEDURES

Chemicals and Reagents. MES was purchased from Sigma. Ethylene glycol, DMSO, sucrose, sodium sulfate, and calcium chloride (anhydrous pellets) were purchased from Baker. Anhydrous sodium acetate, calcium sulfate, and calcium hydroxide were purchased from Fisher Chemical. Calcium acetate, glacial acetic acid, and sodium chloride were purchased from Mallinckrodt. PPBQ and potassium ferricyanide were purchased from Aldrich. All were used without further purification. Stock solutions of PPBQ (25 mM in DMSO) and potassium ferricyanide (100 mM in deionized water) were prepared and frozen until use.

PSII Sample Preparation. PSII membranes were isolated from market spinach leaves following the procedure of Berthold et al. (*52*) with the modifications of Beck et al. (*53*) except that thylakoid membranes were not frozen before isolation of the PSII membranes. The membranes were stored at 77 K in resuspension buffer, containing 15 mM NaCl, 20 mM MES (pH 6.0), and 30% (v/v) ethylene glycol, at concentrations of approximately 6−8 mg of chl mL^{-1} until they were used. PSII membranes provided by George Cheniae were stored at 77 K in buffer, containing 15 mM NaCl, 5 mM $MgCl_2$, 20 mM MES (pH 6.2), and 0.4 M sucrose, prior to being used. Manganese-depleted PSII was prepared by hydroxylamine treatment, as described by Tamura and Cheniae (*54*). Chlorophyll concentrations were measured according to the method of Arnon (*55*) on a Perkin-Elmer Lambda 3b UV/Vis spectrophotometer. Assays for O_2 evolution were carried out in a home-built water-jacketed aluminum chamber maintained at 25 °C by a circulating water bath. Typical O_2 evolution rates were 350−500 μmol of O_2 (mg of chl)$^{-1}$ h^{-1} for untreated PSII as measured by a YSI Clark electrode using light from a 1200 W xenon lamp (Oriel) filtered through a 10 cm water filter, a heat-absorbing filter (Schott KG-5), and a long-pass filter (Oriel LP 610).

Steady-state O_2 evolution assays were performed in a series of 0.6 M ionic strength assay buffers with varied acetate and chloride concentrations. The buffers were prepared as follows. Calcium (20 mM) and sodium (535 mM) were added as hydroxide salts. Acetic acid was added to give acetate concentrations of 0, 20, 100, 250, and 500 mM, and HCl was added to give chloride concentrations of 0, 2, 5,

10, 20, and 55 mM. In each case, the ionic strength was adjusted to 0.6 M by adding the appropriate concentration of MES to bring the pH to 6.0. In the 0.6 M ionic strength buffer without added acetate or chloride, PSII was found to retain 85% of the activity found in buffer containing 20 mM MES (pH 6.0), 20 mM $CaCl_2$, and 15 mM NaCl. All activities determined in the 0.6 M ionic strength buffers were scaled to this value. PSII was added to each buffer and incubated at room temperature for 10−15 min before illumination. Activity assays performed after incubation times varying between 30 s and 30 min showed that, at all acetate and chloride concentrations, the samples reached equilibrium with the added salts within 10 min. While Lindberg and Andréasson showed that in intact PSII centers the exchange of chloride into and out of its site occurs on the order of hours (*7*, *56*), in our experiments much higher chloride concentrations were used (up to 55 mM, as compared to <0.5 mM) which would promote faster exchange. Furthermore, the high ionic strength (0.6 M) of our assay buffers caused partial dissociation of the 17 and 23 kDa extrinsic polypeptides (*57*), as indicated by the sodium dodecyl sulfate−polyacrylamide gel electrophoresis of PSII samples incubated for 30 min in each assay buffer (results not shown). In intact PSII, these extrinsic polypeptides act as a diffusion barrier to anions, and their removal leads to an effective faster exchange of anions into and out of the chloride-binding site. To ensure that the extent of binding of the 17 and 23 kDa extrinsic polypeptides was equivalent in each sample, all buffers were adjusted to the same ionic strength. Each data point represents the average of three measurements.

EPR acetate titration experiments were performed using separate samples for each acetate concentration. Matched samples were prepared from a homogeneous batch of PSII membranes. The membranes were washed once with a buffer containing 40 mM MES (pH 5.5), 0.3 M sucrose, 10 mM calcium acetate, and 1 mM NaCl. They were then resuspended in the same buffer containing either 0, 40, 100, 230, 480, or 730 mM sodium acetate, and 1 or 10 mM chloride was added from a NaCl stock solution (1 M NaCl in a buffer containing 40 mM MES, 0.3 M sucrose, and 10 mM calcium acetate). Each sample was pelleted and resuspended to a concentration of 8−10 mg of chl mL^{-1}. The samples were incubated in the dark at 0 °C for 30−60 min and frozen to 77 K in the dark. Samples for room-temperature EPR measurements were prepared with the same protocol, except that the first washing step was omitted and no chloride was added to the samples with a chloride concentration of <1 mM. Potassium ferricyanide (2 mM) was added to all room-temperature EPR samples, and 500 μM PPBQ was added to all samples prior to use. For room-temperature EPR measurements, samples were centrifuged into a custom-built Wilmad TE quartz flat cell with a fused bottom. Illuminations were performed with a quartz halogen lamp. The $Q_A^-Fe^{II}$ and S_2-state multiline EPR signals were produced by continuous illumination (700 W/m^2) for 5 min in a 200 K bath (dry ice/acetone slurry), followed by rapid cooling in the dark to 77 K. The $S_2Y_Z^\bullet$ EPR signal was produced by continuous illumination (700 W/m^2) for 5 s at room temperature (294 K), followed by rapid freezing in the dark to 77 K. For measurement of light-induced EPR signals at room temperature, samples were illuminated (500 W/m^2) for 30 s during data acquisition.

Analysis of Kinetic Data. Values for K_{Cl} were calculated from fits to plots of activity versus chloride concentration, to Lineweaver−Burk plots at 0 mM acetate, and to a replot of the slopes of the Lineweaver−Burk plots obtained with varied acetate concentrations. The data in all of the Lineweaver−Burk plots were fit simultaneously using Microsoft Excel, by constraining all linear fits to intersect at a single point, while both the intercepts and slopes of the linear fits were allowed to vary. Unconstrained fits gave comparable results and errors. Values for K_I were calculated from a replot of the slopes of the Lineweaver−Burk plots, and from a replot of the slopes of the Dixon plots. The value for K_I was then verified by using it as a constraint in fitting the data in the Dixon plots. A value for K_I' was obtained from a replot of the *y*-intercepts of the Lineweaver−Burk plots. It was verified by using it as a constraint in fitting the data in the Cornish−Bowden plots. The errors in the constrained fits to the Dixon and Cornish−Bowden plots were comparable to those observed in unconstrained fits. The global fit of the data in the Lineweaver−Burk plots with the constraint that all the linear fits intersect at a single point yielded a well-defined error minimum, while in the case of the Dixon and Cornish−Bowden plots, similar global fits did not converge as tightly.

EPR Measurements. Low-temperature EPR measurements were performed on a Varian E-line EPR spectrometer equipped with a TE_{102} cavity and an Oxford Instruments ESR 900 liquid helium cryostat and interfaced with a Macintosh IIci computer. Spectra of the $Q_A^-Fe^{II}$, S_2-state multiline, and $S_2Y_Z^\bullet$ EPR signals were collected under the following conditions: microwave frequency, 9.28 GHz; microwave power, 10 mW; magnetic field modulation frequency, 100 kHz; magnetic field modulation amplitude, 20 G; and temperature, 8 K. The spectra were scaled to the rhombic iron EPR signal at $g = 4.3$. The intensities of the broad $S_2Y_Z^\bullet$ and the S_2-state $g = 4.1$ EPR signals were estimated as peak-to-trough heights in the illuminated-minus-dark difference spectra. The S_2-state multiline EPR signal intensity was approximated as the sum of four to eight hyperfine peak heights in the illuminated-minus-dark difference spectra. For the $Q_A^-Fe^{II}$ EPR signal, the peak height of the sharp feature at $g \approx 1.8$ was measured.

Room-temperature continuous-wave (CW) and time-dependent EPR spectra were collected on a Bruker ER 200D EPR spectrometer equipped with a TM_{110} cavity and interfaced with a Macintosh IIci computer. CW spectra were collected under the following conditions unless noted otherwise: microwave frequency, 9.68 GHz; microwave power, 5.1 mW; magnetic field modulation frequency, 100 kHz; and magnetic field modulation amplitude, 4 G. The formation and decay of the $Y_D^\bullet$ and $Y_Z^\bullet$ EPR signals were monitored as the transient evolution of the low-field hyperfine peak at 3450 G. Time-dependent spectra were collected under the same conditions as the CW spectra, with an instrumental time constant of 0.2 s and a data acquisition rate of 1.0 Hz. The intensities of the narrow $Y_Z^\bullet$ and $Y_D^\bullet$ CW EPR signals were calculated by double integration of the CW spectra. Signal intensities were also approximated as the absolute heights of the derivative EPR signal at 3450 G in the time-dependent EPR spectra.

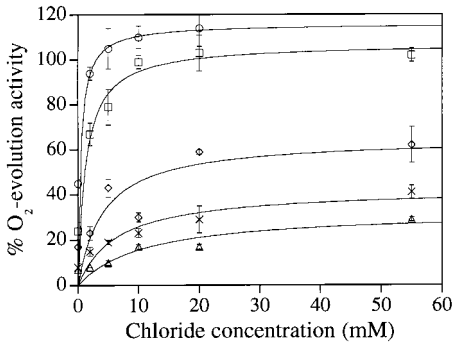

FIGURE 1: Percent O_2 evolution activity as a function of chloride concentration in the presence of (○) 0, (□) 20, (◇) 100, (×) 250, or (△) 500 mM acetate. The data were fit to the Michaelis−Menten equation [rate/V_{max} = [chloride]/(K_{Cl} + [chloride])].

RESULTS

Inhibition of O_2 Evolution. Past studies of the effects of ions on the PSII donor side have reported that O_2 evolution activity of PSII is inhibited in the presence of acetate (*29*, *30*, *34*, *58*). From these results, acetate has been assumed to compete with chloride for a site on or near the Mn_4 cluster. Sandusky and Yocum (*30*) sampled two different chloride concentrations before drawing this conclusion; in other investigations, fixed chloride concentrations were used. However, to obtain a clearer picture of the competition between acetate and chloride in PSII, a range of both chloride and acetate concentrations must be examined. Figure 1 shows that, in the presence of increasing concentrations of acetate, O_2 evolution activity decreases even if optimal chloride concentrations (10−55 mM) are present in the assay chamber. It also shows that even without added chloride 10−40% of the O_2 evolution activity is retained, which is consistent with the results of Lindberg and Andréasson (*11*). As acetate is added, the O_2 evolution activity decreases until it is less than 15% of the initial value, suggesting that acetate renders PSII centers incapable of full O_2 evolution activity by suppressing the effective chloride concentration at or near the Mn_4 cluster.

The type of inhibitory relationship between acetate and chloride can be determined by steady-state enzyme kinetic data analysis (*30*−*32*, *59*). Figure 2A shows a Lineweaver−Burk plot of the data depicted in Figure 1. The lines intersect above the negative *x*-axis, which is indicative of linear mixed competitive inhibition (*59*). In linear mixed competitive inhibition, the overall binding affinity of the inhibitor changes depending on whether the substrate is bound to the enzyme. This change in affinity can be indicative of a change in the inhibitor binding site upon substrate docking. Alternatively, it can indicate the existence of two types of inhibitor binding sites, one of which is substrate-sensitive and the other of which is not, as is the case for ammonia binding to PSII (*31*, *32*). It is known that acetate binds both to the OEC at the donor side, thereby blocking turnover in the $S_2Y_Z^{\bullet}$ state (*20*−*22*), and to the non-heme iron at the acceptor side, thereby slowing the efficiency of Q_A^--to-Q_B electron transfer (*40*, *45*, *46*, *48*). Therefore, the most likely explanation for the mixed linear inhibition of chloride binding by acetate is that acetate binds to two sites, one chloride-sensitive on the OEC and one chloride-insensitive near the non-heme iron.

Dissociation constants K_{Cl} (for chloride binding), K_I (for acetate binding in competition with chloride), and K_I' (for acetate binding that is independent of chloride) are defined in eqs 1−3 and can be calculated from a plot of the slopes and *y*-intercepts of the Lineweaver−Burk plot versus the acetate concentration (Figure 2B; *60*).

$$K_{Cl} = \frac{[PSII][Cl^-]}{[PSII{\cdot}Cl^-_{site1}]} \quad (1)$$

$$K_I = \frac{[PSII][OAc^-]}{[PSII{\cdot}OAc^-_{site1}]} \quad (2)$$

$$K_I' = \frac{[PSII][OAc^-]}{[PSII{\cdot}OAc^-_{site2}]} \quad (3)$$

The characteristics of Dixon (*61*) and Cornish−Bowden (*62*) plots provide alternative means of calculating the values of K_I and K_I'. Their linear fits intersect with an ordinate of $-K_I$ in the Dixon plot and $-K_I'$ in the Cornish−Bowden plot. These plots for acetate inhibition in PSII are shown in panels C and D of Figure 2, respectively. The values calculated for K_{Cl}, K_I, and K_I' are 0.5 ± 0.2, 16 ± 5, and 130 ± 40, respectively (Table 1). As expected, K_{Cl} is much smaller than the acetate dissociation constants. While O_2 evolution activity measurements provide information about the type of inhibition and binding sites, they do not allow specific assignment or structural characterization of the binding sites. To address these issues, EPR measurements on specific redox species within the inhibited PSII samples were conducted.

EPR Characterization of Acetate Inhibition. To link the O_2 evolution inhibition results presented above with specific binding sites on the donor and acceptor sides of PSII, EPR spectra were collected as a function of acetate concentration at ≤1 and 10 mM chloride. Figure 3 shows 200 K illuminated-minus-dark difference EPR spectra, which exhibit the S_2-state multiline and $Q_A^-Fe^{II}$ EPR signals, at selected acetate concentrations and 1 or 10 mM chloride (panels A and B of Figure 3, respectively). The yield of the $Q_A^-Fe^{II}$ EPR signal at $g \approx 1.8$ increases as a function of acetate concentration but is unaffected by chloride (Figure 3C). We conclude that the acceptor side is the site of chloride-insensitive acetate binding in PSII. Acetate binding to the acceptor side is consistent with the finding that other carboxylic acids, such as glycolate, pyruvate, and oxalate, bind to the non-heme iron to produce the $g \approx 1.8$ form of the $Q_A^-Fe^{II}$ EPR signal at concentrations similar to those used here for acetate (*44*−*46*). In addition, acetate and chloroacetates have been identified as inhibitors of Q_A^--to-Q_B electron transfer, further indicating an acceptor side effect (*40*, *48*). When the data in Figure 3C are fit with a Michaelis−Menten type equation for fractional inhibition (eq 4), the value of K_I' is found to be 85 ± 15 mM. This value is the same within error as the value obtained from steady-state O_2 evolution measurements (Table 1).

$$\text{fractional inhibition} = \frac{[OAc^-]}{K_I' + [OAc^-]} \quad (4)$$

In addition to the $Q_A^-Fe^{II}$ EPR signal, the charge separation at 200 K produces the S_2-state multiline and $g = 4.1$ EPR signals from the Mn_4 cluster; it has been shown that the presence of sucrose in the buffers causes both the S_2-state

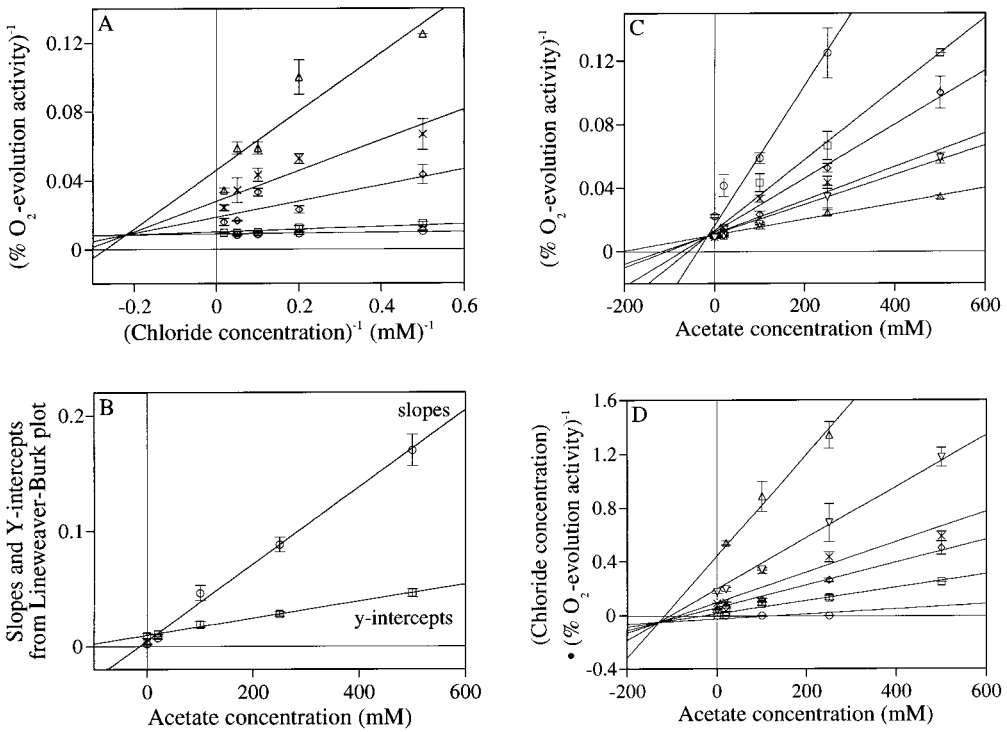

FIGURE 2: (A) Lineweaver−Burk plot of the data from Figure 1 in the presence of (○) 0, (□) 20, (◇) 100, (×) 250, or (△) 500 mM acetate. (B) Replot of the (○) slopes and (□) *y*-intercepts of the plots in panel A. (C) Dixon plot of acetate inhibition of PSII at (○) 0, (□) 2, (◇) 5, (×) 10, (▽) 20, or (△) 55 mM chloride. (D) Cornish−Bowden plot of acetate inhibition of PSII at (○) 0, (□) 2, (◇) 5, (×) 10, (▽) 20, or (△) 55 mM chloride. The solid lines are linear least-squares fits to the data which were calculated as described in Experimental Procedures.

Table 1: Summary of Analyses of Binding Constants[a]

plot type	K_{Cl} (mM)	K_I (mM)	K_I' (mM)
rate vs [chloride]			
0 mM acetate	0.47 ± 0.93		
Lineweaver−Burk ($rate^{-1}$ vs $[chloride]^{-1}$)			
0 mM acetate	0.47 ± 0.03		
all acetate concentrations	0.49 ± 0.15	15 ± 5	130 ± 40
Dixon ($rate^{-1}$ vs [acetate])		17 ± 4	
$Q_A^-Fe^{II}$ EPR signal vs [acetate]			85 ± 15

[a] Lineweaver−Burk, Dixon, and Cornish−Bowden plots (panels A, C, and D of Figure 2, respectively) and EPR data (Figure 3C) were used to determine binding constants and the type of inhibition that was observed. Details on how these values were calculated are provided in Experimental Procedures.

multiline and $g = 4.1$ EPR signals to be formed by 200 K illumination (*63*). The observation of these S_2-state EPR signals is indicative of uninhibited centers, where chloride is bound to the OEC. The yields of both the S_2-state multiline (Figure 3D) and $g = 4.1$ EPR signals (panels A and B of Figure 3) decrease as the concentration of acetate is raised. The effect of acetate on these signals is modulated by chloride, as is demonstrated by the lower yields of the S_2-state multiline EPR signal from samples containing 1 mM chloride than from those containing 10 mM chloride (Figure 3D). At the highest acetate concentration examined (750 mM), neither sample exhibits significant amounts of the S_2-state EPR signals, because no S-state turnover is possible at 200 K when the concentration of acetate is high enough to displace chloride completely (Figure 3A,B, spectra c). When the OEC cannot advance, cytochrome b_{559} acts as the electron donor to $P680^+$ (*64*); the g_z and g_y turning points of photooxidized cytochrome b_{559} are labeled in Figure 3A. Samples containing 1 mM chloride produce higher yields of photooxidized cytochrome b_{559} than samples containing 10 mM chloride (*64*) at equivalent acetate concentrations (Figure 3A,B, spectra b). Photooxidation of cytochrome b_{559} at 200 K is an additional indication that electron transfer from the OEC is impaired. Together, these findings indicate the presence of a chloride-sensitive site for acetate binding at the donor side.

Under room-temperature illumination, acetate-inhibited samples can undergo two turnovers before they become inhibited in the $S_2Y_Z^\bullet$ state (*21*). This state exhibits a characteristic 240 G-wide $S_2Y_Z^\bullet$ EPR signal centered at $g = 2$ at cryogenic temperatures, and a narrow $Y_Z^\bullet$ EPR signal at room temperature. These two EPR signals have been shown to arise from the same species (*26*, *27*). We have used both low- and room-temperature EPR to study the effects of acetate and chloride on the steady-state kinetics of electron-transfer processes leading to formation of the $S_2Y_Z^\bullet$ state and the yields of the associated EPR signals.

To characterize the kinetics of formation and decay of the $S_2Y_Z^\bullet$ state, we monitored the intensity of the light-induced $Y_Z^\bullet$ EPR signal at room temperature. Figure 4 shows the intensity of the low-field tyrosine radical peak as a function of time during illumination, along with the room-temperature CW spectra recorded before, during, and after illumination (spectra a−c, respectively). A significant amount of dark-stable $Y_D^\bullet$ is present in the dark-adapted samples (spectrum a), as is generally observed in intact PSII membranes (*65*). In dark-adapted samples, the tyrosine radical EPR signals from $Y_D^\bullet$ and $Y_Z^\bullet$ form with single-exponential kinetics under room-temperature illumination (Figure 4). The formation rates of $Y_D^\bullet$ and $Y_Z^\bullet$ are indistinguishable because redox equilibration between Y_D and Y_Z is fast on the time scale of kinetic data acquisition (*66*). The same rates of tyrosine

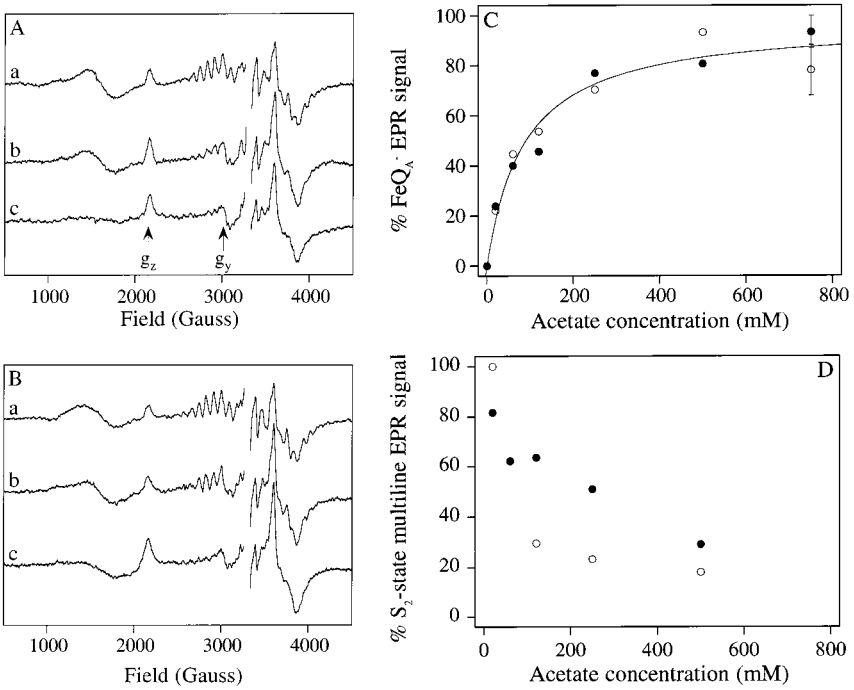

FIGURE 3: 200 K illuminated-minus-dark difference EPR spectra measured at 8 K of PSII treated with (A) 1 or (B) 10 mM chloride and (a) 60, (b) 250, or (c) 750 mM acetate. Arrows indicate the g_z and g_y turning points of the cytochrome b_{559} EPR signal. (C) Yield of the $g \approx 1.8$ $Q_A^-Fe^{II}$ EPR signal as a function of acetate concentration in the presence of (○) 1 or (●) 10 mM chloride. The error bars represent the average of two experiments. The solid line is a least-squares fit of the data to eq 4. (D) Yield of the S_2-state multiline EPR signal as a function of acetate concentration in the presence of (○) 1 or (●) 10 mM chloride.

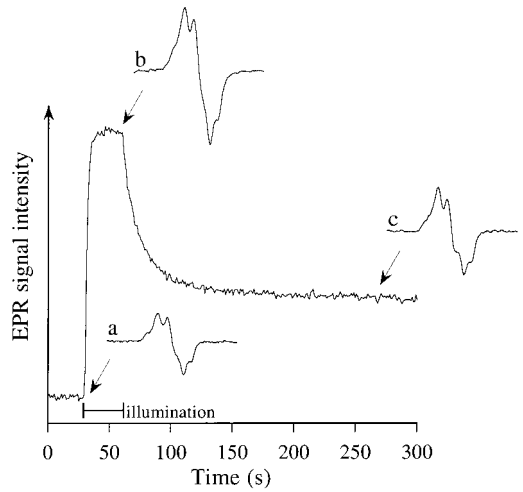

FIGURE 4: Light-induced transient tyrosyl radical EPR signal measured at room temperature in a PSII sample containing 750 mM acetate and 10 mM chloride. Representative pre- and post-illuminated CW spectra (spectra a and c, respectively) as well as the CW spectrum collected during illumination (spectrum b) are included. Magnetic field position, 3450 G.

radical formation are observed independent of the dark adaptation time following acetate and/or chloride treatment (data not shown), indicating that the system is fully equilibrated in the dark. Under continuous saturating illumination at room temperature, a steady state is established within 10−15 s (Figure 4).

While a steady state is established within 10−15 s under room-temperature illumination, a 5 s room-temperature illumination has been found to produce the maximum yield of the cryogenic $S_2Y_Z^\bullet$ EPR signal (*21*). Samples treated with acetate and 1 mM chloride and illuminated for 5 s at room temperature produce higher $S_2Y_Z^\bullet$ EPR signal yields than samples containing 10 mM chloride and equivalent acetate concentrations (Figure 5A,B). A portion of the signal appears to be lost during freezing, leading to fractional intensities that are lower than those observed from $Y_Z^\bullet$ at room temperature (compare Figures 5C and 6B). The effect of chloride on the acetate-induced formation of the $S_2Y_Z^\bullet$ EPR signal (Figure 5C) may be due to chloride-dependent differences in the steady-state yield and/or differences in the rate at which the steady state is approached (see the discussion of Figure 7 below).

To differentiate between these two interpretations, the effects of chloride on the rate of formation and steady-state yield of the $Y_Z^\bullet$ EPR signal in acetate-inhibited PSII were measured at room temperature. A typical room-temperature illuminated-minus-dark difference spectrum of the $Y_Z^\bullet$ EPR signal is shown in Figure 6A. Figure 6B shows the steady-state yields of $Y_Z^\bullet$ as a function of acetate concentration. The steady-state yield of $Y_Z^\bullet$ levels off at about 60% of the fully induced, dark-stable $Y_D^\bullet$ yield. The same observation was recently reported by Babcock and co-workers (*26*). Light saturation experiments were performed to ensure that this effect was not due to nonsaturating illumination conditions (data not shown). Competing pathways for $Y_Z^\bullet$ reduction, such as electron transfer from exogenous reductants, cytochrome b_{559}, or Y_D (*66*), may account for the missing 40% of the $Y_Z^\bullet$ yield in the steady state under saturating illumination conditions at high acetate concentrations. The same yields of $Y_Z^\bullet$ were observed at both <1 and 10 mM chloride (Figure 6B), indicating that the steady-state yield of $Y_Z^\bullet$ depends primarily on chloride-independent acetate effects on the acceptor side turnover. The samples used in the O_2 evolution activity measurements are much more dilute than the EPR samples, and have a significantly higher effective concentration of the exogenous electron acceptor,

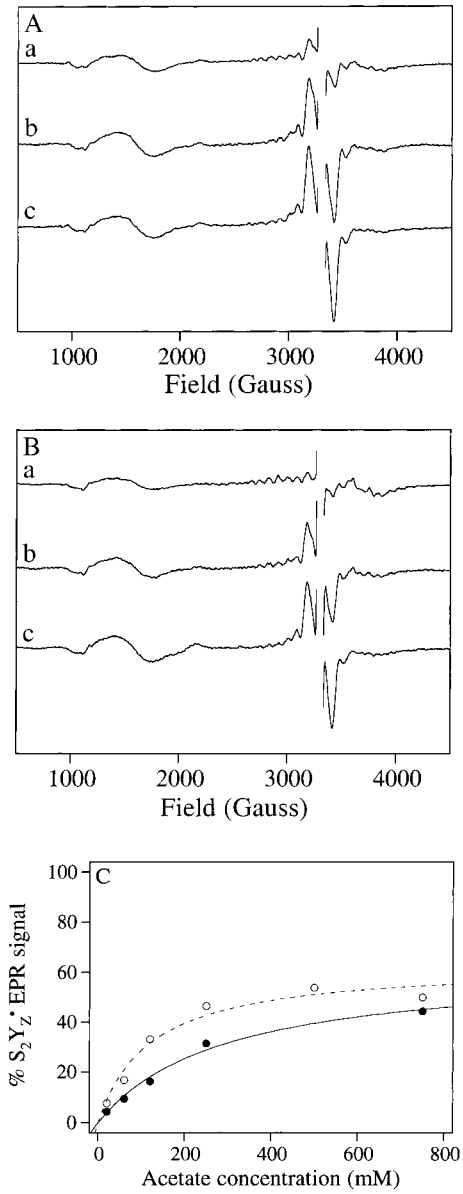

FIGURE 5: Room-temperature illuminated-minus-dark difference EPR spectra measured at 8 K of PSII treated with (A) 1 or (B) 10 mM chloride in the presence of (a) 60, (b) 250, or (c) 750 mM acetate. All spectra are represented on the same *y*-scale. (C) Yield of the $S_2Y_Z^\bullet$ EPR signal as a function of acetate concentration in the presence of (○) 1 or (●) 10 mM chloride. The lines are least-squares fits of the data to eq 4, yielding dissociation constants of (- - -) 120 ± 30 at 1 mM chloride and (—) 300 ± 60 at 10 mM chloride.

PPBQ. In addition, the high viscosity of the EPR samples may limit diffusion of PPBQ into the Q_B site. Consequently, turnover in the EPR samples is likely to be more acceptor side-limited.

In contrast to the steady-state yield of the $Y_Z^\bullet$ EPR signal, its rate of formation depends on both acetate and chloride concentrations (Figure 7). When the chloride concentration in O_2-evolving PSII samples is high, the rate of $Y_Z^\bullet$ EPR signal formation in the presence of acetate is comparable to that in acetate-free Mn-depleted PSII. Because the donor side effect of acetate is eliminated in Mn-depleted PSII, we attribute the effect of acetate in O_2-evolving PSII samples at high chloride concentrations to inhibition of electron transfer on the acceptor side. However, for O_2-evolving PSII

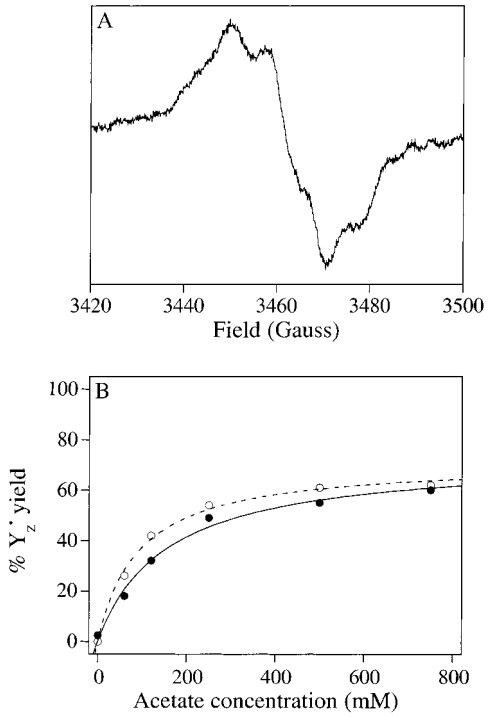

FIGURE 6: (A) Representative illuminated-minus-dark EPR spectrum of $Y_Z^\bullet$ measured at room temperature in a PSII sample containing 500 mM acetate and <1 mM chloride. Microwave power, 10.2 mW; magnetic field modulation amplitude, 2 G. (B) Steady-state yields of the $Y_Z^\bullet$ EPR signal observed at room temperature under illumination as a function of acetate concentration in the presence of (○) <1 or (●) 10 mM chloride. All yields are scaled to the full, dark-stable $Y_D^\bullet$ yield. The lines are least-squares fits of the data to eq 4, yielding dissociation constants of (- - -) 90 ± 10 at <1 mM chloride and (—) 150 ± 30 at 10 mM chloride.

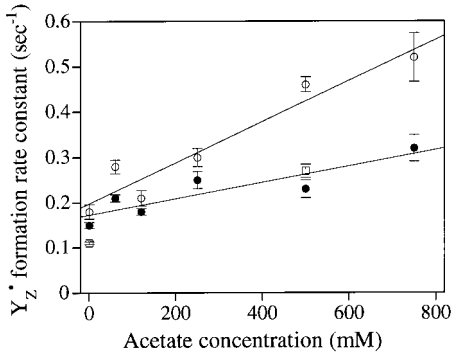

FIGURE 7: $Y_Z^\bullet$ EPR signal formation rates during illumination at room temperature as a function of acetate concentration at (○) <1 or (●) 10 mM chloride in O_2-evolving PSII and at (□) <1 mM chloride in manganese-depleted PSII. The lines are linear least-squares fits of the data.

samples with low chloride concentrations, the rate of formation of the $Y_Z^\bullet$ EPR signal depends on both acetate and chloride concentrations. These results demonstrate that the rate of $Y_Z^\bullet$ formation is affected by chloride-dependent acetate binding to the OEC.

Following continuous illumination at room temperature, the $Y_Z^\bullet$ EPR signal decays biexponentially within about 30 s. While the rates of $Y_Z^\bullet$ EPR signal decay are unaffected by chloride and acetate (data not shown), the percentage of centers in which the $Y_Z^\bullet$ EPR signal forms and then decays at different rates varies with acetate concentration (Figure 8). The fraction of centers that exhibit fast $Y_Z^\bullet$ EPR signal

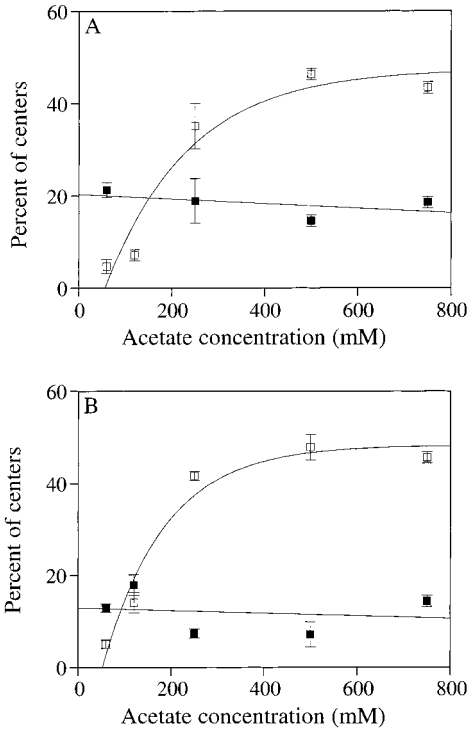

FIGURE 8: Fast and slow phases of $Y_Z^\bullet$ EPR signal decays measured at room temperature. (A) Percentage of centers exhibiting (■) fast or (□) slow $Y_Z^\bullet$ EPR signal decay in the presence of <1 mM chloride. (B) Percentage of centers exhibiting (■) fast or (□) slow $Y_Z^\bullet$ EPR signal decay in the presence of 10 mM chloride. Yields are scaled to the full, dark-stable $Y_D^\bullet$ yield. The lines are (■) linear or (□) exponential least-squares fits of the data.

decay is constant for all acetate and chloride concentrations that are sampled. In contrast, the fraction of centers that exhibit slow $Y_Z^\bullet$ EPR signal decay increases as the acetate concentration is raised. The slow $Y_Z^\bullet$ decay exhibited by these additional inhibited centers may be due to electrostatic stabilization of $Y_Z^\bullet$ by acetate. The invariant percentage of centers that exhibit fast $Y_Z^\bullet$ decay kinetics indicates that there is a separate population of PSII that is incapable of S-state advance and not susceptible to acetate inhibition. It is possible that these centers have been damaged during sample preparation and that the damaging effect is more pronounced in the absence of the stabilizing effects of chloride.

DISCUSSION

We have employed both steady-state O_2 evolution activity and EPR measurements to characterize the binding of acetate and chloride to PSII. Together, our results indicate that two distinct sites for acetate binding exist, one chloride-sensitive and the other chloride-insensitive. We assign the chloride-sensitive acetate-binding site to the donor side of PSII because the rates at which the $S_2Y_Z^\bullet$ and $Y_Z^\bullet$ EPR signals form during room-temperature illumination, as well as the yield of the S_2-state EPR signals produced by 200 K illumination, are found to be both acetate- and chloride-dependent. The chloride-insensitive acetate-binding site is assigned to the acceptor side of PSII, on the basis of the observation that the acetate-induced formation of the $g \approx 1.8$ $Q_A^-Fe^{II}$ EPR signal is independent of the chloride concentration. Our observations can be fully explained by a simple, two-site model, as outlined in Scheme 1. This model incorporates results on Q_A^--to-Q_B electron transfer, which

Scheme 1: Model of Acetate (OAc^-) and Chloride (Cl^-) Binding to a Chloride-Sensitive Site on the Donor Side (DS), and Acetate Binding to a Chloride-Insensitive Site on the Acceptor Side (AS) of PSII, Where DS and AS Correspond to Sites 1 and 2, Respectively, in eqs 1−3

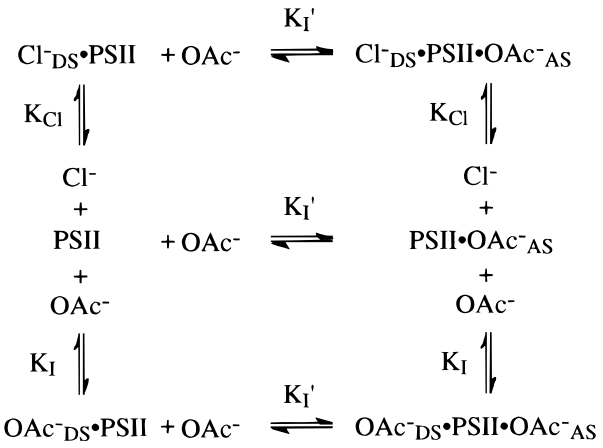

is slowed in the presence of acetate (*40*, *46*−*49*), $Q_A^-Fe^{II}$ EPR signal g value shifts (*44*), presumably caused by bicarbonate displacement (*40*, *49*), and donor side effects of acetate, which lead to $S_2Y_Z^\bullet$ EPR signal formation (*20*, *21*). The dissociation constants associated with each step are given in Table 1.

Recently, Lindberg and Andréasson proposed that chloride binds to the Mn_4 cluster at a high-affinity, slowly exchanging site which can be converted to a low-affinity, rapidly exchanging site with a dissociation constant of 0.5 mM (*11*). Chloride-depleted samples prepared by high-pH sulfate treatments or high-salt washes exhibit chloride dissociation constants of >1 mM and require high levels of external chloride for optimal O_2 evolution activity (*8*, *9*, *67*). This effect probably arises from the loss of the 17 and 23 kDa extrinsic polypeptides, which control the chloride affinity in PSII (*4*). The ionic strengths of the assay buffers used in our study were relatively high, and the 17 and 23 kDa exetrinsic polypeptides may have been partially or fully dissociated (*57*). In fact, SDS−PAGE revealed that the 17 and 23 kDa polypeptides were not present in the acetate-washed PSII samples that were used for EPR measurements (results not shown and ref *68*) and were partially dissociated in the acetate-treated samples that were used for activity assays (results not shown). Activity data taken after incubation times varying between 30 s and 30 min showed that the binding of acetate and chloride had reached equilibrium within 10 min, consistent with the 17 and 23 kDa polypeptides being dissociated under the assay conditions. The dissociation of the 17 and 23 kDa extrinsic polypeptides should make the site more accessible to both chloride and acetate. These results and the chloride dissociation constant of about 0.5 mM obtained from O_2 evolution measurements (Table 1) are in good agreement with chloride binding to the low-affinity site characterized by Lindberg and Andréasson (*11*).

A thorough characterization of the chloride-binding site is necessary for determining the role of chloride in water oxidation. X-ray absorption measurements (*3*) and steady-state O_2 evolution studies (*11*, *30*−*32*) are consistent with direct ligation of chloride to the Mn_4 cluster. If ligated

directly to manganese, chloride may play a mediating role in electron transfer and possibly proton abstraction from substrate bound to the Mn_4 cluster (*69*). While chloride usually acts as a terminal ligand, it can adopt a μ_3-bridging mode in some Mn_4 model complexes (*70*) and a μ_2-bridging chloride has been suggested for the Mn_4 cluster of PSII (*3*, *13*, *31*, *69*). Direct ligation to a transition metal would equally favor binding of anions (such as chloride and acetate) and Lewis bases (such as ammonia) and allow competitive binding of both kinds of species.

Ammonia, fluoride, and small primary amines all bind to the OEC in competition with chloride (*30*−*32*). Given that the size of acetate is comparable to that of chloride, while ammonia is slightly smaller, these inhibitors probably compete for the same site rather than physically precluding chloride binding. Sandusky and Yocum have suggested that replacement of chloride is driven by basicity effects (*30*). Their results indicate that the pK_a of an inhibitory amine is directly proportional to its pK_I, implying that the ability of these inhibitors to compete with chloride is contingent on their adopting a basic form. The pK_a of acetic acid (4.76) is lower than the pK_a of NH_4^+ (9.2) or any of the amines examined by Sandusky and Yocum (*30*). A comparison of the K_I of acetate (16 mM, Table 1) to the K_I of ammonia [0.4 mM (*30*)] shows that the two bases possess very different affinities for the chloride-sensitive binding site in PSII. In fact, the K_I for acetate is significantly higher than the K_I values of all but one of the amines surveyed by Sandusky and Yocum (*30*), indicating that the acetate's inefficiency at replacing chloride in PSII may indeed be attributed to its low pK_a. According to the basicity argument, acetate inhibition should be equally effective at any pH above its pK_a. This is not the case, however, as the $S_2Y_Z^\bullet$ intermediate in acetate-inhibited PSII is observed at pH 6.0 but not at pH >6.5 (*68*). One explanation of the pH dependence of acetate inhibition of S-state turnover is that it reflects the ionization state of ionizable amino acid groups at or near the chloride-binding site. Alternatively, the pH dependence of acetate binding may stem from the fact that it can bind as a bidentate species and may affect other coordination sites in addition to the chloride site.

Acetate-treated samples exhibit the characteristics of chloride-depleted PSII, in which the S_2 state exhibits the $g = 4.1$ instead of the multiline EPR signal (*11*, *12*, *21*, *34*), and S-state advancement is blocked in the $S_2Y_Z^\bullet$ state (*13*, *17*−*19*, *21*, *27*). In addition, acetate-inhibited samples behave like calcium-depleted samples, in that the temperature for the S_1-to-S_2 transition is higher than in intact PSII (*23*, *71*). These findings suggest that acetate binding perturbs both the chloride- and calcium-binding sites, possibly by adopting a binding mode similar to that observed in the Mn(II)−Ca(II) center of concanavalin A (Con A, Figure 9). Con A contains a monodentate bridging carboxylate with a Mn−Ca distance of 4.2 Å, as indicated by X-ray crystallographic studies (*72*, *73*). Extended X-ray absorption fine structure (EXAFS) measurements of PSII have been modeled with a Mn−Ca distance 3.4 Å (*74*). However, this interpretation is controversial (*75*). Penner-Hahn and co-workers have proposed a Mn−Ca distance of 4.3 Å based on EXAFS analyses and have suggested that Con A may provide a model for a Mn−Ca species in the OEC (*76*). The binding modes of the carboxylate groups in Con A may also provide a model for

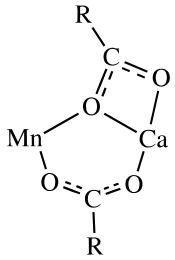

FIGURE 9: Mode of binding of carboxylate groups to the Mn(II)−Ca(II) center in concanavalin A (adapted from ref *79*).

the binding of acetate to the OEC. A mixed-mode binding of acetate to the OEC could account for the effects of acetate inhibition. These effects, which combine those of both chloride and calcium depletion, may stem from the competitive displacement of chloride by acetate together with disruption of the calcium site. Calcium has been proposed to play a key role in substrate water binding to the OEC (*77*), and it is possible that acetate may prevent binding of the substrate by coordinating to an additional site on either manganese or calcium.

Our results support a picture of the water oxidation site of PSII in which the Mn_4 cluster, Y_Z, calcium, and chloride are all in close proximity. EPR spectroscopic studies and spectral simulations of the $S_2Y_Z^\bullet$ EPR signal yield a $Y_Z^\bullet$−Mn_4 distance of 7.5−8.5 Å (*24*, *25*, *28*). This distance is consistent with a structural model in which Y_Z is hydrogen bonded to a substrate molecule bound to Mn, as has been proposed in several recent mechanistic models (*18*, *69*, *78*). In addition, recent $^1H/^2H$ ESEEM results for the acetate-induced $S_2Y_Z^\bullet$ intermediate using acetate labeled on the methyl group have shown that acetate binds in close proximity to $Y_Z^\bullet$ (*22*). Together with our results showing that acetate binds to the OEC in competition with chloride, we deduce that chloride also binds close to Y_Z. Altogether, these results lead to the conclusion that both chloride and $Y_Z^\bullet$ are proximal to the Mn_4 cluster. Future studies of acetate-inhibited PSII may yield a refined structural model of the OEC and insight into the roles of both chloride and calcium in water oxidation chemistry.

ACKNOWLEDGMENT

We thank Dr. George Cheniae (University of Kentucky, Lexington, KY) for the generous gift of untreated PSII membranes. We also thank Drs. R. David Britt and Gerald Babcock for providing manuscripts prior to publication.

REFERENCES

1. Kok, B., Forbush, B., and McGloin, M. (1970) *Photochem. Photobiol. 11*, 457−475.
2. Debus, R. J. (1992) *Biochim. Biophys. Acta 1102*, 269−352.
3. Yachandra, V. K., DeRose, V. J., Latimer, M. J., Mukerji, I., Sauer, K., and Klein, M. P. (1993) *Science 260*, 675−679.
4. Homann, P. H. (1987) *J. Bioenerg. Biomembr. 19*, 105−123.
5. Yocum, C. F. (1991) *Biochim. Biophys. Acta 1059*, 1−15.
6. Diner, B. A., and Babcock, G. T. (1996) in *Oxygenic Photosynthesis: The Light Reactions* (Ort, D., and Yocum, C., Eds.) pp 213−247, Kluwer Academic Publishers, Dordrecht, The Netherlands.
7. Lindberg, K., Wydrzynski, T., Vänngård, T., and Andréasson, L.-E. (1990) *FEBS Lett. 264*, 153−155.
8. Homann, P. H. (1985) *Biochim. Biophys. Acta 809*, 311−319.
9. Miyao, M., and Murata, N. (1985) *FEBS Lett. 180*, 303−308.

10. Homann, P. H. (1988) *Photosynth. Res. 15*, 205−220.
11. Lindberg, K., and Andréasson, L.-E. (1996) *Biochemistry 35*, 14259−14267.
12. Beck, W. F., and Brudvig, G. W. (1988) *Chem. Scr. 28A*, 93−98.
13. Wincencjusz, H., van Gorkom, H. J., and Yocum, C. F. (1997) *Biochemistry 36*, 3663−3670.
14. Baumgarten, M., Philo, J. S., and Dismukes, G. C. (1990) *Biochemistry 29*, 10814−10822.
15. Boussac, A., Sétif, P., and Rutherford, A. W. (1992) *Biochemistry 31*, 1224−1234.
16. van Vliet, P., and Rutherford, A. W. (1996) *Biochemistry 35*, 1829−1839.
17. Hallahan, B. J., Nugent, J. H. A., Warden, J. T., and Evans, M. C. W. (1992) *Biochemistry 31*, 4562−4573.
18. Gilchrist, M. L., Lorigan, G. A., and Britt, R. D. (1995) *Proc. Natl. Acad. Sci. U.S.A. 92*, 9545−9549.
19. Tang, X.-S., Randall, D. W., Force, D. A., Diner, B. A., and Britt, R. D. (1996) *J. Am. Chem. Soc. 118*, 7638−7639.
20. MacLachlan, D. J., and Nugent, J. H. A. (1993) *Biochemistry 32*, 9772−9780.
21. Szalai, V. A., and Brudvig, G. W. (1996) *Biochemistry 35*, 1946−1953.
22. Force, D. A., Randall, D. W., and Britt, R. D. (1997) *Biochemistry 36*, 12062−12070.
23. Szalai, V. A., and Brudvig, G. W. (1996) *Biochemistry 35*, 15080−15087.
24. Dorlet, P., Di Valentin, M., Babcock, G. T., and McCracken, J. L. (1998) *J. Phys. Chem. B 102*, 8239−8247.
25. Lakshmi, K. V., Eaton, S. S., Eaton, G. R., Frank, H. A., and Brudvig, G. (1998) *J. Phys. Chem. B 102*, 8327−8335.
26. Lydakis-Simantiris, N., Dorlet, P., Ghanotakis, D. F., and Babcock, G. T. (1998) *Biochemistry 37*, 6427−6435.
27. Szalai, V. A., Kühne, H., Lakshmi, K. V., and Brudvig, G. W. (1998) *Biochemistry 37*, 13594−13603.
28. Peloquin, J. M., Campbell, K. A., and Britt, R. D. (1998) *J. Am. Chem. Soc. 120*, 6840−6841.
29. Sinclair, J. (1984) *Biochim. Biophys. Acta 764*, 247−252.
30. Sandusky, P. O., and Yocum, C. F. (1986) *Biochim. Biophys. Acta 849*, 85−93.
31. Sandusky, P. O., and Yocum, C. F. (1983) *FEBS Lett. 162*, 339−343.
32. Sandusky, P. O., and Yocum, C. F. (1984) *Biochim. Biophys. Acta 766*, 603−611.
33. Damoder, R., Klimov, V. V., and Dismukes, G. C. (1986) *Biochim. Biophys. Acta 848*, 378−391.
34. Ono, T., Nakayama, H., Gleiter, H., Inoue, Y., and Kawamori, A. (1987) *Arch. Biochem. Biophys. 256*, 618−624.
35. Kelley, P. M., and Izawa, S. (1978) *Biochim. Biophys. Acta 502*, 198−210.
36. Critchley, C., Baianu, I. C., Govindjee, and Gutowsky, H. S. (1982) *Biochim. Biophys. Acta 682*, 436−445.
37. Michel, H., and Deisenhofer, J. (1988) *Biochemistry 27*, 1−7.
38. Stemler, A., and Govindjee (1973) *Plant Physiol. 52*, 119−123.
39. Khanna, R., Govindjee, and Wydrzynski, T. (1977) *Biochim. Biophys. Acta 462*, 208−214.
40. Blubaugh, D., and Govindjee (1988) *Photosynth. Res. 19*, 85−128.
41. Diner, B. A., and Petrouleas, V. (1990) *Biochim. Biophys. Acta 1015*, 141−149.
42. Petrouleas, V., and Diner, B. A. (1990) *Biochim. Biophys. Acta 1015*, 131−140.
43. Koulougliotis, D., Kostopoulos, T., Petrouleas, V., and Diner, B. A. (1993) *Biochim. Biophys. Acta 1141*, 275−282.
44. Petrouleas, V., Sanakis, Y., Deligiannakis, Y., and Diner, B. A. (1992) in *Current Research in Photosynthesis* (Murata, N., Ed.) Vol. II, pp 119−122, Kluwer Academic Publishers, Dordrecht, The Netherlands.
45. Deligiannakis, Y., Petrouleas, V., and Diner, B. A. (1994) *Biochim. Biophys. Acta 1188*, 260−270.
46. Petrouleas, V., Deligiannakis, Y., and Diner, B. A. (1994) *Biochim. Biophys. Acta 1188*, 271−277.
47. Bock, C. H., Gerken, S., Stehlik, D., and Witt, H. T. (1988) *FEBS Lett. 227*, 141−146.
48. Govindjee, Chunhe, X., Schansker, G., and van Rensen, J. J. S. (1997) *J. Photochem. Photobiol. 37*, 107−117.
49. Vermaas, W. F. J., and Rutherford, A. W. (1984) *FEBS Lett. 175*, 243−248.
50. Beck, W. F., and Brudvig, G. W. (1986) *Biochemistry 25*, 6479−6486.
51. Boussac, A., Rutherford, A. W., and Styring, S. (1990) *Biochemistry 29*, 24−32.
52. Berthold, D. A., Babcock, G. T., and Yocum, C. F. (1981) *FEBS Lett. 134*, 231−234.
53. Beck, W. F., de Paula, J. C., and Brudvig, G. W. (1985) *Biochemistry 24*, 3035−3043.
54. Tamura, N., and Cheniae, G. (1987) *Biochim. Biophys. Acta 890*, 179−194.
55. Arnon, D. I. (1949) *Plant Physiol. 24*, 1−15.
56. Lindberg, K., Vänngård, T., and Andréasson, L.-E. (1993) *Photosynth. Res. 38*, 401−408.
57. de Paula, J. C., Li, P. M., Miller, A.-F., Wu, B. W., and Brudvig, G. W. (1986) *Biochemistry 25*, 6487−6494.
58. Saygin, Ö., Gerken, S., Meyer, B., and Witt, H. T. (1986) *Photosynth. Res. 9*, 71−78.
59. Segel, I. H. (1993) *Enzyme Kinetics: Behavior and Analysis of Rapid Equilibrium and Steady-State Enzyme Systems*, Wiley-Interscience, New York.
60. Szalai, V. (1998) Ph.D. Thesis, Yale University, New Haven, CT.
61. Dixon, M. (1953) *Biochem. J. 55*, 170−171.
62. Cornish-Bowden, A. (1974) *Biochem. J. 137*, 143−144.
63. Miller, A.-F., and Brudvig, G. W. (1991) *Biochim. Biophys. Acta 1056*, 1−18.
64. Thompson, L. K., and Brudvig, G. W. (1988) *Biochemistry 27*, 6653−6658.
65. Buser, C. A., and Brudvig, G. A. (1992) in *Research in Photosynthesis* (Murata, N., Ed.) Vol. II, pp 85−88, Kluwer Academic Publishers, Dordrecht, The Netherlands.
66. Buser, C. A., Thompson, L. K., Diner, B. A., and Brudvig, G. W. (1990) *Biochemistry 29*, 8977−8985.
67. Homann, P. H. (1988) *Biochim. Biophys. Acta 934*, 1−13.
68. MacLachlan, D. J., Nugent, J. H. A., Warden, J. T., and Evans, M. C. W. (1994) *Biochim. Biophys. Acta 1188*, 325−334.
69. Limburg, J., Szalai, V. A., and Brudvig, G. W. (1999) *J. Chem. Soc., Dalton Trans.*, 1353−1363.
70. Wang, S., Tsai, H.-L., Libby, E., Folting, K., Streib, W. E., Hendrickson, D. N., and Christou, G. (1996) *Inorg. Chem. 35*, 7578−7589.
71. Ono, T., and Inoue, Y. (1990) *Biochim. Biophys. Acta 1020*, 269−277.
72. Hardman, K. D., Agarwal, R. C., and Freiser, M. J. (1982) *J. Mol. Biol. 157*, 69−86.
73. Lin, S.-L., Stern, E. A., Kalb, A. J., and Zhang, Y. (1990) *Biochemistry 29*, 3599−3603.
74. Latimer, M. J., DeRose, V. J., Mukerji, I., Yachandra, V. K., Sauer, K., and Klein, M. P. (1995) *Biochemistry 34*, 10898−10909.
75. Riggs-Gelasco, P. J., Mei, R., Ghanotakis, D. F., Yocum, C. F., and Penner-Hahn, J. E. (1996) *J. Am. Chem. Soc. 118*, 2400−2410.
76. Penner-Hahn, J. E., Fronko, R. M., Pecoraro, V. L., Yocum, C. F., and Betts, S. D. (1990) *J. Am. Chem. Soc. 112*, 2549−2557.
77. Rutherford, A. W. (1989) *Trends Biochem. Sci. 14*, 227−232.
78. Hoganson, C. W., and Babcock, G. T. (1997) *Science 277*, 1953−1956.
79. Rardin, R. L., Tolman, W. B., and Lippard, S. J. (1991) *New J. Chem. 15*, 417−430.

BI990341T